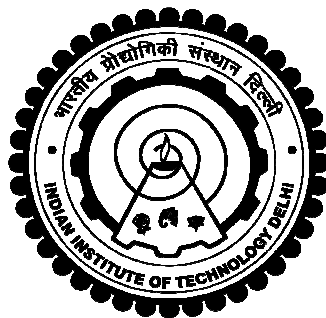


DESIGN OF WIRELINE COMMUNICATION RECEIVERS FOR MULTI-GIGABIT DATA RATES

SUSHRANT MONGA



**DEPARTMENT OF ELECTRICAL ENGINEERING
INDIAN INSTITUTE OF TECHNOLOGY DELHI
AUGUST 2016**

**DESIGN OF WIRELINE COMMUNICATION
RECEIVERS FOR MULTI-GIGABIT DATA RATES.**

by

(SUSHRANT MONGA)

Department of Electrical Engineering

Submitted

in fulfillment of the requirements of the degree of

Doctor of Philosophy

to the



Indian Institute of Technology Delhi

August 2016

Certificate

This is to certify that the thesis entitled “*Design of wireline communication receivers for multi-gigabit data rates.*”, being submitted by **Mr. Sushrant Monga** to the Indian Institute of Technology Delhi, is worthy of consideration for the award of the degree of **Doctor of Philosophy** and is a record of the original bonafide research work carried out by him under my guidance and supervision. The results contained in the thesis have not been submitted in part or full, to any other University or Institute for the award of any degree or diploma.

I certify that he has pursued the prescribed course of research.

Dr. Kaushik Saha

Director,

Samsung R&D Institute India

Delhi

Dr. Shouri Chatterjee

Associate Professor,

Department of Electrical Engineering

Indian Institute of Technology Delhi

Hauz Khas, New Delhi – 110016

Date:

New Delhi

Acknowledgments

I express my deep heartfelt gratitude to my respected parents, Mrs. Sushma Monga and Mr. Sudershan Monga for their blessings and patience which allowed me to pursue this research. I am indebted to their unconditional support all through my tenure as a research scholar without which it would have been impossible to complete my work. Thanks to my sister who encouraged me and cheered me to achieve my goals. I am thankful to my wife who motivated me and kept along during my work.

I express my gratitude to, Dr. Shouri Chatterjee, who kept his faith in me and always enhanced my research-abilities throughout the course of learning from him.

I thank my research committee members Prof. Ananjan Basu, Prof. Basabi Bhaumik and Prof. G.S.Visweswaran for their useful inputs. A special thanks to Prof. Brejesh Lall for free ranging discussions on various topics. I would like to thank Gajendranath Chaudhary, Hitesh Shrimali, Avikal Bansal for their support on technical writing skills, system configuration and software support for various tools time and again.

– Sushrant Monga

Abstract

Contributions to the architecture and modeling of high speed serial link transceivers are presented in this thesis. Basically three contributions are described that address the issues of jitter and intersymbol interference in the receiver at gigabit data rates. Design proposals (modeling and CMOS implementation) specifically for termination impedance at the transmitter and the receiver, equalizer and clock and data recovery circuits for gigabit receiver are presented.

The thesis presents an adaptive transmitter designed in 40 nm CMOS that calibrates its termination impedance to the characteristic impedance of the channel that ensures a low Bit Error Rate (BER) across external variables independent of operating conditions (process, voltage and temperature). The design presents digital calibration of the termination over an impedance range of 30Ω - 120Ω with an accuracy of ($\leq 8 \%$). These digital calibration codes are also distributed to the receiver for the calibration of receiver's termination assuming the common architecture for the impedance design. The calibration scheme enables the transmitter to function as a plug-n-play device across multiple environments. Mathematical formulation for the problem of impedance matching in practical scenarios is presented thereby developing the proposed solution for dynamic impedance calibration. Simulation results for the implemented system are presented showing the respective waveforms with a total power consumption for the receiver to be 20 mW @2.5 V in contrast to other reported results.

A single tap CMOS continuous-time feedback equalization is proposed as a solution to

solve the latency issues in decision feedback equalization (DFE). The architecture avoids the use of synchronous blocks having a continuous feedback loop with controlled transconductance in the feedback path that gives the required delay for the desired operation of the loop. The equalizer is designed in 130 nm CMOS and is scalable across technologies. The measurement results show effective equalization with little area and power overhead. Post-simulation and measurement results indicate a minimum equalization gain (for the default setting of the digital calibration in the equalizer) of 5 dB(min.) at a frequency of 2.98 Ghz (almost 3 Ghz) for data rates approaching 6 Gb/s.

In this thesis a clock and data recovery (CDR) architecture is presented to enhance the jitter tolerance to the input data thus ensuring a lower BER for multiple data rates. A hybrid architecture with open-loop and closed-loop clock recovery schemes is presented. The results for the behavioral model for the CDR show high jitter tolerance for the input with random jitter (RJ= 2.264 ps) in addition to the deterministic jitter (DJ= 30 ps pk-pk) superimposed with the sinusoidal jitter components such that the total data jitter reaches 64% of the data-eye. The clock trajectory (in time) for the behavioral model of the proposed CDR is shown respect to the state-of-art CDR's (open-loop and closed loop recovery architectures). The simulation results for CMOS 65nm design are presented for the input data having $RJ=0.01 U I_{rms}$ and $DJ = 0.2 U I_{pp}$. Simulation results are also presented for the input data (to the CDR) having only the residual ISI (output of the cascade of the channel and CTFE) and no other source of jitter to show the functioning of the respective blocks.

Contents

List of Figures	iii
List of Tables	xi
1 Design challenges for high speed serial link receivers	1
1.1 Introduction	1
1.2 Decision Feedback Equalization	9
1.3 Clock and Data Recovery	14
2 Designing receivers for adaptability to the external variables	27
2.1 Introduction	28
2.2 Problem Definition	28
2.3 Mathematical Formulation	33
2.4 Description	38
2.5 Design	41
2.5.1 Driver	44
2.5.2 Receiver	45
2.5.3 Calibration Block	48
2.6 Results	51

2.7	Conclusions	51
3	Design of an tunable inductorless analog front-end of the receiver	53
3.1	Introduction	54
3.2	Problem Description	56
3.3	Design	65
3.4	Results	72
3.5	Conclusions	83
4	High jitter tolerant programmable data recovery technique	85
4.1	Introduction	86
4.2	Architecture Description	91
4.3	Oversampling Clock Recovery	95
4.4	Modelling Results	109
4.5	Conclusions	113
5	Design of an tunable inductorless gigabit receiver with an enhanced jitter tolerance	
	CDR	115
5.1	Design	115
5.1.1	Receiver Architecture	115
5.2	Simulation Results	126
5.3	Conclusions	140
6	Conclusions and future scope	141

List of Figures

1.1	Cross-sectional view of the backplane channel indicating different sections of the signaling path between two mounted linecards.	2
1.2	Variable degradation for different channels in backplane (S_{21} parameter plot). <i>Source: [1].</i>	3
1.3	Pulse response @8 Gb/s for a 26 inch channel.	4
1.4	A model of a typical backplane channel.	5
1.5	Spectrum of an ideal (zero rise and fall times) random data-bit stream.	5
1.6	Model of the serial-link showing the interface to the digital transmission and reception.	6
1.7	Impulse response for a channel with brick-wall filter response and a model for a low-pass channel with -3dB point at a frequency less than f_s	6
1.8	ISI for a channel modelled as a LPF showing the precursor and the post-cursor contributions in time.	7
1.9	Response of the channel, equalizer, and the combined response of the channel augmented by the equalizer.	8
1.10	(a) DFE implementation with the feedback filter. (b) Specific case of 1-bit Current mode CMOS DFE implementation.	10

1.11	(a) Block diagram for a full-rate 1-tap CMOS DFE implementation. (b) Block diagram for a 1-tap half-rate CMOS DFE implementation. (c) 1-tap speculative or loop unrolled DFE.	13
1.12	(a) Waveform eye diagrams from different jitter distributions (EYE A and EYE B have the same jitter eye opening at TJ = 10-12). (b) Statistical distribution of the received signal vs receiver phase, FR4 baseline for PAM2 signal at 3.125 Gb/s. <i>Source: PCI Express Jitter Modeling, Revision 1.0 RD</i>	15
1.13	Classical Analog PLL based CDR.	16
1.14	Jitter Tolerance and Jitter transfer curves for the charge pump PLL based CDR.	18
1.15	Mathematical model for the digital loop based CDR.	19
1.16	Block Diagram for the DPLL.	20
1.17	Loop transfer for the linearized model of the D/PLL.	21
1.18	Block level schematic of Dual Loop CDR.	22
1.19	Top-level schematic of the clock recovery proposed [2].	23
1.20	Clock recovery scheme for the oversampling CDR.	24
1.21	Limitation of the over-sampled CDR.	25
2.1	A typical communication system at physical layer abstraction showing the signalling link (single-ended).	29
2.2	Modes of operation for the I/O buffer on the time scale.	31
2.3	Ideal resistor driving a loss-less channel with capacitive termination at the far-end.	32
2.4	(a) Simulation results for the output voltage 3σ process variation with $Z_C=30$ ohms, $Z_D=50$ ohms. (b) Simulation results for the output voltage for $Z_C=30$ ohms 120 ohms, $Z_D=50$ ohms at the typical process corner.	33
2.5	The push-pull driver.	34

2.6	Modeling for the driver-channel interface.	34
2.7	Span of the rise/fall time at the PAD for the calibration range of the drive impedance.	36
2.8	Timing margin for sampling the data for different Z_c	38
2.9	Strategy for the delay calibration.	40
2.10	Top level architecture for the proposed transceiver consisting of the I/O buffer and calibration block.	41
2.11	Architecture for the pull-up branch of the output drive stage (ODS)	42
2.12	Impedance calibration scheme for the proposed I/O buffer with unknown line's impedance.	43
2.13	Transistor level architecture for the proposed driver.	44
2.14	Top level block diagram for the receiver.	46
2.15	Circuit diagram for the Sample and Hold Block.	46
2.16	PAD output voltage with relation to sampling edges and the pre-driver signals.	47
2.17	Conceptual schematic for the emulated impedance (EI) block.	47
2.18	Simulation results for the adaptive driver showing various signals during sampling phase.	48
2.19	Impedance Calibration phase with top level signals at the output driver and calibration block.	50
3.1	Active feedback technique showing adaptive control of the input transconductance stage.	54
3.2	Decision feedback equalization.	56
3.3	1-tap loop-unrolled DFE implementation.	57

3.4	(a) Transfer gain of 1-Tap DFE with slicer. (b) Eye diagram at the output of 1-Tap DFE without slicer. (c) Eye diagram at the output of 1-Tap DFE with slicer.	58
3.5	Analogy to the full rate DFE to derive the proposed architecture.	60
3.6	Analog summation in the current domain for high speed DFE.	61
3.7	Simplified diagram showing the functionality of the proposed system with signal waveforms at different nodes.	63
3.8	Block diagram of the CTFE architecture.	63
3.9	Signal Flow of the gain boost strategy implemented in the receiver.	64
3.10	The incoming data stream with random pattern having equal probability for '1' and '0'.	64
3.11	Top level schematic highlighting the loop delay constraint.	64
3.12	Simplified schematic for the summing node of the feedback loops.	65
3.13	Circuit diagram for AC analysis of the system.	66
3.14	Schematic of the bias control between the input and the feedback transconductance.	67
3.15	Half circuit description of the modified Cherry-Hooper amplifier.	68
3.16	Model of the equalizer for calculating the transfer function.	70
3.17	S-domain model for the amplifier.	70
3.18	The S21 parameter plot vs. frequency for the channel used for simulations.	73
3.19	The figure shows the top-level schematic used for circuit simulations in CMOS 130 nm.	73
3.20	Simulation plots for the input voltage to the receiver after passing through the channel (see Fig. 3.1), the voltage at the summer (mixing nodes O and OB) and the output of the amplifier (refer Fig. 3.1).	75

3.21	Schematic for 1-tap speculative DFE implemented in 130 nm CMOS.	76
3.22	Waveforms at the highlighted interface nodes of 1-tap speculative DFE shown in Fig. 3.21.	77
3.23	Waveforms at the highlighted intermediate nodes of 1-tap speculative DFE shown in Fig. 3.21.. . . .	78
3.24	Eye diagram at the input of the receiver (simulation).	78
3.25	Eye diagram at the output of the receiver (post-layout simulation).	78
3.26	Photo-micrograph of the fabricated chip showing the proposed equalizer.	79
3.27	Test set-up for the measuring the S-parameters of the equalizer using Network analyzer.	79
3.28	(a) Measured S-parameters for the CTFE. (b) Transfer function $\frac{OUT}{INP}$ calculated from the measured S-parameters.	81
3.29	(a) Simulated S-parameters for the CTFE. (b) Transfer function $\frac{OUT}{INP}$ calculated from the simulated S-parameters.	82
4.1	Clock derived for various CDR schemes.	86
4.2	Jitter tolerance mask specified for the SERDES for 10G Ethernet.	87
4.3	Loop based CDR architecture.	88
4.4	Jitter transfer function for the critically damped phase tracking CDR based on SONET OC-3 specifications. (<i>Source: SONET OC3 specifications</i>)	89
4.5	Jitter tolerance curve for the tracking CDR.	89
4.6	Gated oscillator based CDR architecture.	90
4.7	Sinusoidal jitter tolerance of the GRO-based CDR.	91
4.8	Eye-diagram showing jitter at the data crossovers. The voltage uncertainty in- creases at sample locations away from the ideal sampling position.	92

4.9	Proposed CDR with oversampling clock recovery and first-order track loop.	92
4.10	Relation of the clock's sampling edge to the abounding data crossovers.	94
4.11	Concept of operation for the proposed oversampling clock recovery.	94
4.12	Proposed oversampling CDR.	95
4.13	Sampling data by four equi-spaced phases of the clock.	96
4.14	Data bit spans an interval of $0 - 180^\circ$ and is phase quantized by the blind clock.	96
4.15	Schematic for 4 DFF's sampled by respective clock phases.	97
4.16	Figure showing sampling and re-timing with phase detection.	98
4.17	Decision boundaries for the in-phase and quadrature clocks.	99
4.18	Schematic for the logic processing block.	100
4.19	"SUB-LOGIC" for individual phase selection.	100
4.20	Figure shows different clock phases selected by their respective enable bits	101
4.21	Top level abstraction for the 'Logic' block.	102
4.22	Figure showing the delay in the data path as quantized into the multiples of clock's phase shift.	103
4.23	Case of long CID's for deriving the control bits.	104
4.24	Simulated BER for different values of frequency error and jitter on clock with CID =5, random jitter(RJ)= $0.015UI_{rms}$, deterministic jitter(DJ) = $0.2UI_{pp}$, $f_B = 2.5 Gb/s$, see [3].	105
4.25	Clocks selected in the 'Operate' block to form the output clock.	106
4.26	Phase interpolation with MUX's controlled by the selection bits.	107
4.27	Phase interpolator's output as a function of two input phases and the control-bit E_{offset}	108
4.28	Data eye showing the ideal sampling point with respect to abounding data edges	110

4.29	Figure highlighting the position of the clock with respect to the ideal sampling position of ‘y=0’ after the settling of the PLL-based clock with a loop bandwidth of 50 MHz.	111
4.30	Model for evaluating the CDR’s performance.	112
4.31	Jitter tolerance for the simulated receiver.	113
5.1	Top-level schematic for the complete receiver showing the proposed equalizer and the CDR.	116
5.2	Design approach for the proposed CDR circuit.	117
5.3	Figure shows different clock phases selected by their respective enable bits . . .	119
5.4	CMOS implementation for the phase interpolator	121
5.5	Top level schematic for the (clk-DLL).	123
5.6	(a) CMOS design strategy for the delay stage with indicative biasing. (b) Design of the delay stage showing the calibration.	124
5.7	CMOS design of the CP + LF for the DLL.	125
5.8	(a) Eye diagram at the input of the equalizer. (b) Eye-diagram at the output of the equalizer.	127
5.9	Figure showing the position of the input data to the BO-CR circuit with respect to the different phases of the half-rate clock used in the BO-CR.	128
5.10	Figure showing the output interface of the LB for logic units each corresponding to the processing for rising and falling edge captured samples.	129
5.11	(a) Simulation result for control voltage for the DLL. (b) Delayed output differential clocks $OUTP_i, OUTM_i$	133
5.12	(a) Control outputs of the LB for positive clock cycle. (b) Control outputs of the LB for negative clock cycle.	134

5.13 (a) Interface signals highlighted for the BO-CR block. (b) Highlighted interface signals that are probed for the "OPERATE" block. 135

5.14 Figure showing the position of the VCDL's output (*INPDELAY*, *INMDELAY*) to the output of the BO-CR circuit *OUTPCLK* and *OUTMCLK*. The signals are shown with respect to clock phases *CLK0*, *CLK45*, *CLK90*, *CLK135* . . . 136

5.15 Top-level diagram of the !!PD highlighting the input/output nodes. 136

5.16 Eye diagram for the data input and output for the !!PD with respect to the data sampling clock (*I_{CLK}*) 137

5.17 Figure shows the test-setup for the clock recovery of the noisy data. 137

5.18 Eye-diagram of the input to the !!PD with respect to the data-sampling phase of the clock (*I_{CLK}*) over 1 UI with $RJ = 0.01 UI_{rms}$, $DJ = 0.2 UI_{pp}$ with UI = 125 ps. 138

5.19 Layout for the receiver with the proposed CDR. 138

5.20 Pie distribution chart for power consumption. 139

List of Tables

1.1	LIST OF PARAMETERS (see Fig. 1.13)	17
2.1	ADAPTIVE IMPEDANCE CALIBRATION FOR THE TRANSMITTER . . .	50
3.1	DESIGN OF CMOS EQUALIZER	80
4.1	LIST OF PARAMETERS	109